Aberystwyth University

Crystal Structure of Schistosoma mansoni Arginase, a Potential Drug Target for the Treatment of Schistosomiasis

Hai, Yang; Edwards, Jennifer; Van Zandt, Michael C.; Hoffmann, Karl Francis; Christianson, David W.

Crystal Structure of *Schistosoma mansoni* Arginase, a Potential Drug Target for the Treatment of Schistosomiasis

Yang Hai,[†] Jennifer E. Edwards,[‡] Michael C. Van Zandt,[§] Karl F. Hoffmann,[‡] and David W. Christianson*,[†]

[†]Roy and Diana Vagelos Laboratories, Department of Chemistry, University of Pennsylvania, Philadelphia, Pennsylvania 19104-6323, United States

[‡]Institute of Biological, Environmental and Rural Sciences, Aberystwyth University, Aberystwyth, Ceredigion SY23 3DA, United Kingdom

[§]New England Discovery Partners, 23 Business Park Drive, Branford, Connecticut 06405, United States

S *Supporting Information*

ABSTRACT: The X-ray crystal structure of arginase from *Schistosoma mansoni* (SmARG) and the structures of its complexes with several amino acid inhibitors have been determined at atomic resolution. SmARG is a binuclear manganese metalloenzyme that catalyzes the hydrolysis of L-arginine to form L-ornithine and urea, and this enzyme is upregulated in all forms of the parasite that interact with the human host. Current hypotheses suggest that parasitic arginases could play a role in host immune evasion by depleting pools of substrate L-arginine that would otherwise be utilized for NO biosynthesis and NO-dependent processes in the immune response. Although the amino acid sequence of SmARG is only 42% identical with that of human arginase I, residues important for substrate binding and catalysis are strictly conserved. In general, classical amino acid inhibitors such as 2(*S*)-amino-6-boronohexanoic acid (ABH) tend to bind more weakly to SmARG than to human arginase I despite identical inhibitor binding modes in each enzyme active site. The identification of a patch on the enzyme surface capable of accommodating the additional Cα substitutent of an α,α-disubstituted amino acid inhibitor suggests that such inhibitors could exhibit higher affinity and biological activity. The structures of SmARG complexed with two different α,α-disubstituted derivatives of ABH are presented and provide a proof of concept for this approach in the enhancement of enzyme−inhibitor affinity.
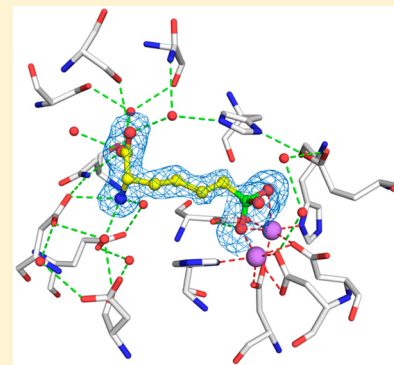
S chistosomiasis, also known as bilharzia or snail fever, is a neglected tropical disease caused by parasitic schistosomes (also known as blood flukes) indigenous to tropical and subtropical regions of the developing world.[1−4] *Biomphalaria* freshwater snails serve as intermediate hosts for *Schistosoma mansoni* and release infectious larvae (cercariae), which burrow into human skin upon contact with contaminated water sources. After definitive host penetration, the parasite transforms into a schistosomulum that enters the circulation and migrates to the hepatic portal and mesenteric veins surrounding the liver. Here, schistosomula develop into sexually mature adults (male and female forms) that can evade immunity and thrive for many years.[5−7] Intravascular adult females produce hundreds of eggs daily during this time, which either cross the intestinal lumen to continue the lifecycle or circulate to the liver where they induce a robust host immunological response.[5] Chronic inflammation of the liver ultimately results, leading to portal vein hypertension and severe hepatic fibrosis. Although schistosomiasis is usually treated effectively with praziquantel, currently believed to target schistosomal voltage-gated Ca^{2+} channels,[8] the continuous threat of praziquantel-resistant schistosomes portends an urgent need for alternative drug targets.[9−12]

The binuclear manganese metalloenzyme arginase may comprise just such an alternative. Although arginase activity was first discovered in *S. mansoni* 50 years ago[13] and implicated in L-proline biosynthesis,[14] *S. mansoni* arginase (SmARG) was not enzymatically characterized until recently.[15] The full-length mRNA for SmARG encodes a 364-residue protein with an amino acid sequence that is 42 and 40% identical with those of human arginases I and II, respectively, which catalyze the hydrolysis of L-arginine to yield L-ornithine and urea (Figure 1a).[16,17] All residues important for catalysis by the human isozymes, including two histidine and four aspartate ligands to the binuclear manganese cluster, are strictly conserved in SmARG. Interestingly, SmARG exhibits a relatively high turnover number of 537 s^{-1}, approximately 2-fold higher than that measured for human arginase II and 20% higher than that reported for human arginase I.[18,19] Using a homology model of SmARG based on the crystal structure of human arginase I,[16] Fitzpatrick and colleagues predicted the formation of a disulfide
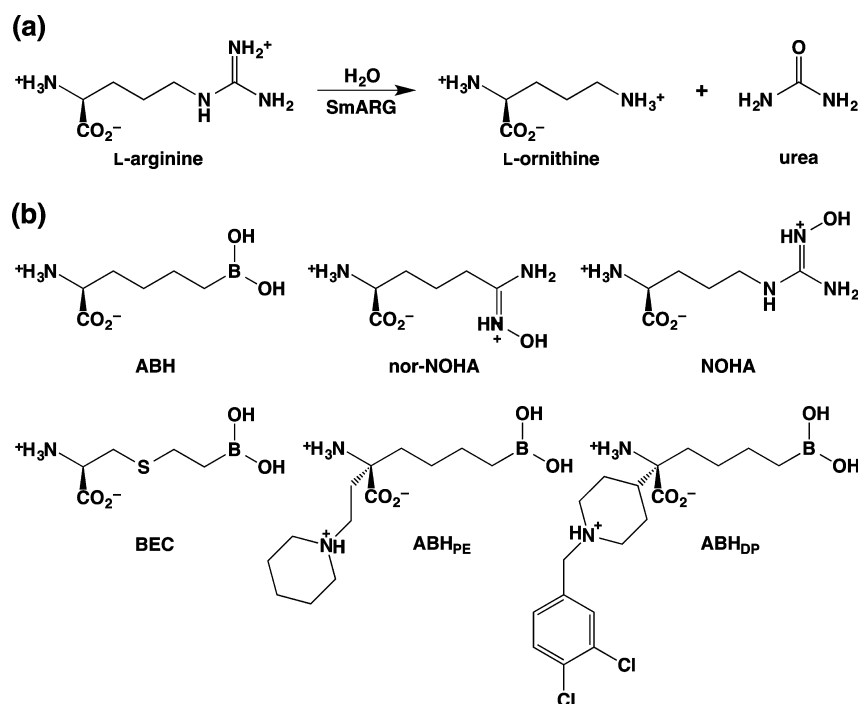
Figure 1. (a) Reaction catalyzed by arginase. (b) Arginase inhibitors 2(*S*)-amino-6-boronohexanoic acid (ABH), *S*-(boronoethyl)-L-cysteine (BEC), *N*-hydroxy-L-arginine (NOHA), nor-*N*-hydroxy-L-arginine (nor-NOHA), (*R*)-2-amino-6-borono-2-[2-(piperidin-1-yl)ethyl]hexanoic acid (ABH$_{PE}$), and (*R*)-2-amino-6-borono-2-[1-(3,4-dichlorobenzyl)piperidin-4-yl]hexanoic acid (ABH$_{DP}$). Although ABH$_{DP}$ is shown as the single stereoisomer that binds to SmARG, the racemic mixture was utilized for the experiments described herein.

linkage between proximal residues C291 and C332 in the active site; the enzyme activity is significantly reduced in the presence of reducing agents, consistent with the potential functional relevance of a disulfide linkage.[15]

SmARG is expressed in all life stages of the parasite that interact with the human host[15] and is hypothesized to play a role in immune evasion. By depleting the L-arginine substrate otherwise utilized for nitric oxide (NO) biosynthesis, SmARG can attenuate the anti-schistosomula NO-mediated immune response of classically activated macrophages.[20] A similar strategy of arginase-facilitated immune evasion is exploited by *Leishmania* parasites in leishmaniasis,[21−23] *Helicobacter pylori* in peptic ulcer disease,[24,25] and certain cancer tumor cells.[26−29] Accordingly, inhibition of SmARG might render the parasite more susceptible to the immune response. If so, then SmARG may comprise a new target for structure-based drug design in the treatment of schistosomiasis.[15]

As the first step in exploring the "druggability" of SmARG, we now report the X-ray crystal structures of the unliganded enzyme and its complexes with selected inhibitors (Figure 1b), including the classical boronic acid amino acid inhibitors 2(*S*)-amino-6-boronohexanoic acid (ABH)[30] and *S*-(boronoethyl)-L-cysteine (BEC).[31] Additionally, we report crystal structures of SmARG complexes with the *N*-hydroxyguanidinium amino acids *N*-hydroxy-L-arginine (NOHA)[32] and nor-*N*-hydroxy-L-arginine (nor-NOHA),[33] as well as the simple amino acids L-ornithine (the catalytic product), L-lysine, and L-valine. Finally, to advance beyond classical amino acid inhibitor designs, we report the crystal structures of SmARG complexed with two novel α,α-disubstituted amino acid derivatives of ABH: (*R*)-2-amino-6-borono-2-[2-(piperidin-1-yl)ethyl]hexanoic acid (ABH$_{PE}$)[34] and (*R*)-2-amino-6-borono-2-[1-(3,4-dichlorobenzyl)piperidin-4-yl]hexanoic acid (ABH$_{DP}$).[35] The additional α-substituents of ABH$_{PE}$ and ABH$_{DP}$ make new

interactions that enhance enzyme−inhibitor affinity. These studies illuminate structure−function relationships relevant to the understanding of catalysis by SmARG and provide a foundation for exploring the design of next-generation inhibitors targeting a distinctive new region of the protein surface.

■ MATERIALS AND METHODS

Materials. Manganese(II) chloride tetrahydrate (≥99%), L-arginine, and α-isonitrosopropiophenone were purchased from Sigma. Tris(2-carboxyethyl)phosphine hydrochloride (98%, TCEP) was purchased from Gold Biotechnology. ABH was purchased from Enzo Life Sciences (Farmingdale, NY). NOHA, nor-NOHA, and BEC were purchased from Cayman Chemical Co. (Ann Arbor, MI). ABH$_{PE}$ and ABH$_{DP}$ were the generous gifts of New England Discovery Partners. A 30% (w/v) PEG 20000 solution, a 50% (w/v) PEG 3350 solution, a 50% (w/v) PEG 10000 solution, and a 100% Tacsimate (pH 7.0) solution were purchased from Hampton Research. All other chemicals were purchased from Fisher Scientific.

Expression and Purification of SmARG. A silent mutation was introduced into the gene encoding wild-type SmARG prepared in a TOPO vector to eliminate a native NdeI site by using the QuickChange method (Stratagene) with the following oligonucleotide primers [sense, 5′-GGT AAT ATG AGT CGG GCG GCA <u>CAC</u> ATG CAG CAG ACA AAA CAA TAA TCG-3′; antisense, 5′-CGA TTA TTG TTT TGT CTG CAT <u>GTG</u> TGC CGC CCG ACT CAT AAT ACC-3′ (underlined bases indicate the silent mutation)]. The coding sequence for SmARG was then amplified by polymerase chain reaction (PCR) using oligonucleotide primers [sense, 5′-GCA GCA <u>CAT ATG</u> ATG TTG AAA TCA GTC GCG ACC-3′; antisense, 5′-GCA GCA <u>CTC GAG</u> TTA TTG TTT TGT CTG CAT GTG TGC-3′ (underlined bases represent the

restriction enzyme recognition sites)]. The PCR product was subcloned into NdeI and XhoI sites of the pET-28a vector (Novagen Inc.), yielding an N-terminal hexahistidine tag, a thrombin cleavage site, and a linker (MGSSHHHHHHSSGL-VPRGSHM). All DNA constructs were verified by DNA sequencing at the Perelman School of Medicine of the University of Pennsylvania.

SmARG was overexpressed in *Escherichia coli* BL21(DE3) cells. Transformed cell cultures were grown in Lysogeny-Broth (LB) medium supplemented with 50 μg/L kanamycin. Expression was induced by 1 mM isopropyl β-D-1-thiogalacto-pyranoside (IPTG) (Carbosynth) for 16 h at 20 °C when the OD_{600} reached 0.6−0.7. Cells were harvested by centrifugation at 6000g for 10 min. The cell pellet was resuspended in buffer A [50 mM K_2HPO_4 (pH 8.0), 300 mM NaCl, 10% (v/v) glycerol, and 1 mM TCEP]. Cells were lysed by sonication on ice using a Sonifer 450 (Branson), and the cell lysate was clarified by centrifugation at 26895g for 1 h. Proteins were isolated from lysate by affinity chromatography with a Talon column (Clontech Laboratories, Mountain View, CA). After being washed with 10 column volumes of 20 mM imidazole in buffer A, SmARG was eluted with a 200 mL gradient from 20 to 300 mM imidazole. Pooled fractions were concentrated and applied to a Superdex 200 preparative grade 26/60 size exclusion column (GE Healthcare) with buffer B [50 mM bicine (pH 8.5) and 100 μM $MnCl_2$]. The estimated purity of SmARG was >95% on the basis of sodium dodecyl sulfate−polyacrylamide gel electrophoresis. Although the N-terminal hexahistidine tag and linker segment contained a thrombin cleavage site, the recombinant enzyme was not treated with thrombin and hence contained a full-length N-terminus. The enzyme was concentrated to 40 mg/mL, flash-frozen with liquid nitrogen, and stored at −80 °C.

The C291A and C332A mutants of SmARG were prepared by PCR mutagenesis with the following primers (underlined bases indicate mutated codons): C291A, 5′-GAA GGT TTG AGA ATA GCT GAA GAA GTT TC-3′ (sense) and 5′-GAA ACT TCT TCA GCT ATT CTC AAA CCT TC-3′ (antisense); C332A, 5′-CAT ATT TTA AGA GCA GCT TTA GGC CAT TGT CG-3′ (sense) and 5′-CGA CAA TGG CCT AAA GCT GCT CTT AAA ATA TG-3′ (antisense). Each mutant was purified as described above for the wild-type enzyme.

Activity Assays. Arginase activity was assayed by a colorimetric assay developed by Archibald with slight modifications.[36] Briefly, 0.5−50 mM L-arginine (pH 8.5) was added to a solution of 50 mM 4-(2-hydroxyethyl)piperazine-1-propanesulfonic acid (EPPS) (pH 8.5) and 100 μM $MnCl_2$, and the reaction was initiated by adding 1 μM SmARG in a total volume of 200 μL at 21 °C. The reaction was terminated after 1 min using 30 μL of a 3:1 (v/v) concentrated acid/dye solution {H_2SO_4/H_3PO_4/H_2O [1:3:1 (v/v/v)] mixture with 245 mM α-isonitrosopropiophenone in ethanol}. Samples were heated to 90 °C for 1 h in a thermocycler to ensure complete reaction of urea with the dye. To quantify urea formation, the absorbance of each sample was assessed at a λ of 550 nm using a Tecan Infinite M1000 Pro Microplate Reader. Kinetic parameters were determined with Graphpad Prism (2008). The K_i values for ABH and NOHA were calculated using the modified Michaelis−Menten equation for competitive inhibition. All measurements were performed in triplicate.

Isothermal Titration Calorimetry (ITC). A MicroCal iTC$_{200}$ calorimeter (GE Healthcare) was used to measure the dissociation constants of SmARG−inhibitor complexes using previously reported procedures.[16,31] Briefly, SmARG was exhaustively dialyzed against 50 mM Bicine (pH 8.5), 100 μM $MnCl_2$, and 1.0 mM TCEP [5% (v/v) DMSO was included in the dialysis buffer when SmARG was titrated with ABH$_{PE}$ and ABH$_{DP}$]. The inhibitor (ABH, 0.547 mM; NOHA, 1.097 mM; nor-NOHA, 0.443 mM; ABH$_{PE}$, 0.410 mM; ABH$_{DP}$, 0.436 mM) was dissolved in dialysis buffer. The inhibitor was titrated into the sample cell (0.2 mL) overfilled with SmARG (typically 20−40 μM) with sequential injections. An initial 0.2 μL injection was not used in the data analysis. Data analysis was performed using Origin version 7.0. For SmARG complexes with nor-NOHA, ABH, ABH$_{PE}$, and ABH$_{DP}$, data were best fit assuming a single binding site. For the SmARG−NOHA complex, data were best fit with the equation describing two sets of independent sites, i.e., a model in which binding to one site (association constant K_1) has a higher affinity than binding to the second site (association constant K_2):

$$Q = [E]_t V \left(\frac{n_1 \Delta H_1 K_1 [L]}{1 + K_1 [L]} + \frac{n_2 \Delta H_2 K_2 [L]}{1 + K_2 [L]} \right)$$

where Q is the heat evolved during the course of the reaction, $[E]_t$ is the total enzyme concentration, V is the cell volume, n_1 is the number of inhibitor equivalents required to saturate the first binding site, n_2 is the number of equivalents to saturate the second site, ΔH_1 and ΔH_2 are the enthalpies per mole of ligand of binding to the first and second sites, respectively, and $[L]$ is the inhibitor concentration. Note that dissociation constants $K_{d1} = 1/K_1$ and $K_{d2} = 1/K_2$.

Crystallography. Unliganded SmARG crystals were prepared by the sitting drop vapor diffusion method at 4 °C. Typically, a 4 μL drop of a protein solution [10 mg/mL SmARG, 50 mM bicine (pH 8.5), and 100 μM $MnCl_2$] was mixed with a 4 μL drop of a precipitant solution [12% (w/v) PEG 20000 and 0.1 M imidazole (pH 7.0)] and equilibrated against a 500 μL reservoir of a precipitant solution. Cubic crystals first appeared after 2 days and grew to maximal size in 3 days. To obtain crystals of the SmARG−L-ornithine, SmARG−L-valine, and SmARG−L-lysine complexes, unliganded SmARG crystals were soaked with each ligand (50 mM) in a 20 μL drop of a soaking solution [14% PEG 20000 and 0.1 M imidazole (pH 7.0)] equilibrated against a 500 μL reservoir of a soaking solution for 24 h. To cocrystallize SmARG with the higher-affinity arginase inhibitors ABH, BEC, NOHA, and nor-NOHA, as well as the α,α-disubstituted amino acid inhibitors ABH$_{PE}$ and ABH$_{DP}$, SmARG was incubated with each inhibitor (10 mM) on ice for 1 h before the crystallization experiment. Typically, a 1 μL drop of protein solution (9 mg/mL SmARG, 45 mM bicine, 90 μM $MnCl_2$, and 10 mM inhibitor) was added to a 1 μL drop of a precipitant solution [4% (v/v) Tacsimate (pH 7.0) and 12% (w/v) PEG 3350 for SmARG−ABH and SmARG−BEC complexes; 0.2 M potassium sodium tartrate tetrahydrate, 0.1 M Bis-Tris (pH 6.5), and 10% (w/v) PEG 10000 for the SmARG−NOHA complex; 0.2 M L-proline, 0.1 M HEPES (pH 7.5), and 10% (w/v) PEG 3350 for the SmARG−norNOHA complex; 0.1 M HEPES (pH 7.4) and 12% (w/v) PEG 3350 for the SmARG−ABH$_{PE}$ complex; and 0.15 M CsCl and 13% (w/v) PEG 3350 for the SmARG−ABH$_{DP}$ complex] and equilibrated against a 100 μL reservoir of a precipitant solution. Cubic crystals appeared overnight and grew to maximal size in 3 days. All crystals were flash-cooled in liquid nitrogen after being transferred to a cryoprotectant

Table 1. Data Collection and Refinement Statistics of SmARG Complexes

	unliganded	ABH	ABH$_{PE}$	ABH$_{DP}$	nor-NOHA	NOHA	BEC	L-ornithine	L-valine	L-lysine
PDB entry	4Q3P	4Q3Q	4Q3S	4Q3R	4Q3U	4Q3T	4Q3V	4Q42	4Q40	4Q41
Data Collection										
space group	$P2_13$	$P2_13$	$P2_13$	$P2_13$	$P2_13$	$P2_13$	$P2_13$	$P2_13$	$P2_13$	$P2_13$
resolution (Å)	2.50	2.00	2.11	2.17	2.50	2.14	2.70	2.05	1.83	2.20
no. of reflections measured (total/unique)	468739/65315	1358593/126488	993349/106363	1704963/96325	382879/61714	599891/102397	198632/51489	1458071/118020	813401/163491	659561/94329
unit cell parameters [$a = b = c$ (Å)]	178.4	178.2	178.2	177.5	178.3	177.8	178.4	178.4	177.8	177.4
completeness^a (%)	99.9 (99.6)	100 (99.9)	98.5 (96.1)	98.3 (92.5)	94.4 (87.0)	99.9 (99.6)	98.8 (99.7)	100 (100)	99.9 (99.9)	100 (100)
$I/\sigma_I{}^a$	13.7 (2.1)	13.5 (3.1)	14.7 (2.0)	16.5 (2.0)	18.2 (2.1)	12.0 (2.0)	10.5 (2.0)	19.2 (3.8)	14.1 (2.1)	13.5 (3.5)
$R_{sym}{}^b$	0.167 (0.834)	0.153 (0.831)	0.106 (0.757)	0.165 (1.190)	0.118 (0.712)	0.150 (0.883)	0.158 (0.655)	0.130 (0.790)	0.099 (0.813)	0.123 (0.667)
$R_{pim}{}^c$	0.066 (0.350)	0.045 (0.262)	0.031 (0.342)	0.041 (0.376)	0.047 (0.412)	0.066 (0.420)	0.088 (0.353)	0.079 (0.175)	0.044 (0.363)	0.037 (0.222)
redundancy	7.2 (6.4)	10.7 (9.8)	9.3 (5.3)	17.7 (10.1)	6.3 (3.6)	5.9 (5.2)	3.9 (3.6)	12.4 (12.4)	5.0 (5.0)	7.0 (7.0)
Refinement										
no. of reflections (refinement/test set)	65276/3303	118487/5927	106337/5301	96490/4812	61299/3100	102353/5117	51451/2636	111704/5586	152572/7678	91351/4574
R_{work}/R_{free} (%)^d	17.7/21.4 (24.7/30.4)	16.8/20.2 (20.1/24.5)	17.3/20.6 (23.2/25.8)	17.4/20.6 (24.9/29.4)	17.4/22.5 (21.7/29.0)	17.6/20.9 (24.8/29.2)	16.7/21.7 (24.1/31.2)	17.4/20.8 (20.4/23.5)	17.4/19.5 (25.5/26.5)	17.2/20.1 (23.5/26.1)
no. of protein atoms^e	10271	10241	10270	10120	10182	10243	10306	10289	10261	10223
no. of solvent atoms	495	895	849	627	390	607	353	679	1019	397
no. of ligand atoms	36	88	132	173	84	127	75	72	109	56
no. of Mn^{2+} ions	8	8	8	8	8	8	8	8	8	8
rmsd										
bonds (Å)	0.005	0.010	0.006	0.009	0.009	0.006	0.005	0.008	0.009	0.009
angles (deg)	0.9	1.2	1.0	1.1	1.2	1.0	0.9	1.1	1.1	1.1
average B factor (Å^2)										
main chain	36	30	30	32	44	29	30	32	27	47
side chain	37	34	33	34	45	32	32	36	31	50
solvent	29	34	33	30	38	30	24	35	33	43
Mn^{2+} ions	29	21	23	24	37	24	25	26	20	37
ligands	37	34	34	45	43	42	32	40	32	52
Ramachandran plot (%)										
allowed	91.4	92.0	92.2	91.4	90.5	92.0	91.4	92.1	91.5	92.0
additionally allowed	8.6	8.0	7.8	8.6	9.5	8.0	8.6	7.9	8.5	8.0
generously allowed	0.0	0.0	0.0	0.0	0.0	0.0	0.0	0.1	0.0	0.0
disallowed	0.0	0.0	0.0	0.0	0.0	0.0	0.0	0.0	0.0	0.0

^{a}Values in parentheses refer to data for the highest-resolution shell. $^bR_{sym} = \sum_h \sum_i |I(h)_i - \langle I(h) \rangle| / \sum_h \sum_i I(h)_i$, where $I(h)$ is the intensity of reflection h, $\sum_h$ is the sum over all reflections, and $\sum_i$ is the sum over i measurements of reflection h. $^cR_{pim} = \sum_h [1/(n-1)]^{1/2} \sum_i |I - \langle I \rangle| / \sum_h \sum_i I$, where n is the number of observations (redundancy) and $\langle I \rangle$ is the average intensity calculated from replicate data. $^dR_{work} = \sum_i ||F_o| - |F_c|| / \sum |F_o|$ for reflections contained in the working set. $R_{free} = \sum ||F_o| - |F_c|| / \sum |F_o|$ for reflections contained in the test set held aside during refinement. $|F_o|$ and $|F_c|$ are the observed and calculated structure factor amplitudes, respectively. ^{e}Per asymmetric unit.

solution consisting of mother liquor supplemented with 15–20% (v/v) glycerol.

X-ray diffraction data were collected on beamline X29 at the National Synchrotron Light Source (NSLS, Brookhaven National Laboratory, Upton, NY). Diffraction data were integrated and scaled with HKL2000.[37] Data collection and reduction statistics are listed in Table 1. All crystals belonged to space group $P2_13$ with four molecules in the asymmetric unit, each belonging to a separate SmARG trimer in the unit cell. The structure of unliganded SmARG was determined by molecular replacement using PHASER[38] as implemented in the CCP4 suite of programs[39] with the atomic coordinates of unliganded human arginase I (PDB entry 2ZAV)[40] utilized as a search probe for rotation and translation function calculations. Iterative cycles of refinement and model building were performed using PHENIX and COOT, respectively.[41,42] The structures of SmARG−inhibitor complexes were determined thereafter by molecular replacement using the atomic coordinates of unliganded SmARG as a search probe. Solvent molecules and inhibitors were added in the final stages of refinement for each structure. The quality of each final model was verified with PROCHECK, and the secondary structure was defined with DSSP.[43,44] Disordered segments excluded from the final models include the N-terminal hexahistidine tag and its linker segment, residues M1−P17, surface loop K111−S119, and T362−Q364 at the C-terminus. Refinement statistics are listed in Table 1. Protein structure figures were prepared with PyMol (http://www.pymol.org) and PhotoshopCS.

SmARG Transcription Profile. Data from the 37632-element *S. mansoni* long-oligonucleotide DNA microarray studies of Fitzpatrick and colleagues[45] were interrogated to find the expression profile of SmARG across 14 different life cycle stages. Raw and normalized fluorescence intensity values are available via Array Express under experimental accession number E-MEXP-2094.

Helminth Fluorescence Bioassay. Mechanically transformed *S. mansoni* schistosomula were treated with the arginase inhibitors ABH (Enzo Life Sciences), NOHA (Sigma), and nor-NOHA (Enzo Life Sciences) at a final concentration of 100 μM and incubated for 24 h at 37 °C in a humidified environment containing 5% CO_2. The viability of *S. mansoni* schistosomula subsequent to treatment was determined using the helminth fluorescence bioassay as previously described.[46] All assays were performed in duplicate.

■ RESULTS

SmARG Transcription Profile. The transcription profile of SmARG across 14 different *S. mansoni* life cycle stages (Figure 2) confirms previously published semiquantitative reverse transcription PCR data showing that SmARG is maximally expressed in all life stages that interact with the definitive mammalian host but minimally expressed in life stages that interact with the intermediate snail host.[45] Thus, the upregulation of SmARG is specific to human infection by *S. mansoni*. If SmARG plays an important role during human infection, it could serve as a new target for the treatment of schistosomal infections.

Activity Assays and ITC Measurements. Our measurements show that wild-type SmARG exhibits a turnover number (k_{cat}) of 330 ± 60 s^{-1} and a K_M value of 12 ± 5 mM at pH 8.5 using Archibald's colorimetric assay[36] to quantify urea production in steady-state kinetic assays (Table 2). These values are in reasonable agreement with previously reported
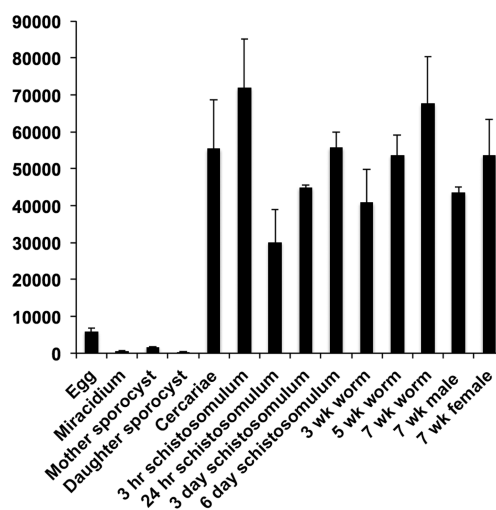

Figure 2. Expression profile of SmARG across 14 different life cycle stages of *S. mansoni* shown following interrogation of the 37632-element DNA microarray. Raw and normalized fluorescence intensity values are available via Array Express under experimental accession number E-MEXP-2094. Histograms represent the normalized mean fluorescence intensity ± the standard deviation of the mean.

values of 537 s^{-1} and 17 mM, respectively, for a slightly different SmARG construct at pH 9.7 containing the remnant of an N-terminal glutathione S-transferase fusion tag[15] instead of the hexahistidine tag and linker utilized herein. These values are also comparable to those measured for human arginase I, although the K_M values of SmARG are slightly larger (4−6-fold) than the K_M value reported for the human enzyme (Table 2).

Steady-state kinetic analysis yields an inhibition constant (K_i) of 1.8 ± 0.6 μM for the SmARG−ABH complex, which is consistent with the ITC measurement of 1.3 ± 0.2 μM for the dissociation constant (K_d) of this complex (Figure S1 of the Supporting Information). Interestingly, ITC measurements indicate 260-fold tighter binding of ABH to human arginase I, but the inhibitory potencies of ABH against SmARG and human arginase I are comparable (Table 2). The origin of the difference between K_i and K_d values is unknown.

ITC measurements indicate that K_d = 0.36 ± 0.08 μM for the SmARG−nor-NOHA complex (Figure S1 of the Supporting Information). The binding of NOHA is slightly more complex, and ITC data are best fit by a model in which the binding affinity for the first site is higher (K_d = 0.33 ± 0.09 μM) than the binding affinity for the second site (K_d = 13 ± 4 μM). The location of the weaker binding site is unknown, because only the higher-affinity binding site is occupied in the crystal structure of the SmARG−NOHA complex (*vide infra*). Taken together, these data suggest that the *N*-hydroxyguanidinium moiety of nor-NOHA is ∼4-fold more effective as an inhibitor functional group targeting metal ion coordination than the tetrahedral boronate anion of ABH in binding to SmARG. This contrasts with human arginase I, which is preferentially inhibited (at least 10-fold) by ABH compared with nor-NOHA.[16,47] Possibly, these selectivity differences (summarized in Table 2) could be exploited in developing inhibitors that preferentially block the parasitic enzyme.

Finally, ITC measurements indicate K_d values of 0.26 ± 0.02 and 0.54 ± 0.08 μM for SmARG−ABH$_{PE}$ and −ABH$_{DP}$ complexes, respectively (Figure S1 of the Supporting Information). Notably, the additional α-substituent of these

Table 2. Enzyme Kinetics and Inhibitor Binding Affinities

	K_M (mM)	k_{cat} (s^{-1})	k_{cat}/K_M (M^{-1} s^{-1})	K_i (ABH) (μM)	K_d (ABH) (μM)	K_i (NOHA) (μM)	K_d (NOHA) (μM)	K_d (nor-NOHA) (μM)	K_d (ABH$_{PE}$) (μM)	K_d (ABH$_{DP}$) (μM)
wild-type SmARG[a]	12 ± 5	330 ± 60	(3.0 ± 0.9) × 10^4	1.8 ± 0.6	1.3 ± 0.2	3.7 ± 0.8	0.33 ± 0.09, 13 ± 4	0.36 ± 0.08	0.26 ± 0.02	0.54 ± 0.08
C291A SmARG[a]	90 ± 10	110 ± 10	(1.2 ± 0.3) × 10^3	nd	nd	nd	nd	nd	nd	nd
C332A SmARG[a]	32 ± 9	100 ± 20	(3.3 ± 0.6) × 10^3	nd	nd	nd	nd	nd	nd	nd
SmARG[b]	17	537	3.2 × 10^4	nd	nd	nd	nd	nd	nd	nd
human arginase I	3 ± 1[c]	340 ± 160[c]	(11 ± 2) × 10^{4c}	3.5[d]	0.005[e]	nd	3.6[f]	0.517[g]	nd	nd

[a]This study; determined by an enzyme assay at pH 8.5. [b]From ref 15; determined by an enzyme assay at pH 9.7. [c]From ref 63; determined by an enzyme assay at pH 8.5. [d]From ref 64; determined by an enzyme assay at pH 9.5. [e]From ref 16; K_d determined at pH 8.5 by isothermal titration calorimetry. [f]From ref 47; K_d determined at pH 8.5 by surface plasmon resonance. [g]From ref 47; K_d determined at pH 8.5 by surface plasmon resonance; however, isothermal titration calorimetry yielded a K_d of ~50 nM.

α,α-disubstituted amino acid inhibitors provides 2−5-fold enhancement of the affinity compared with that of the parent SmARG−ABH complex.

Structure of Unliganded SmARG. The overall fold of the SmARG monomer is generally similar to that of unliganded human aginase I (PDB entry 2ZAV)[40] with an rmsd of 1.1 Å for 271 Cα atoms, which is consistent with the modest amino acid sequence identity of 42% between SmARG and human arginase I. SmARG oligomerizes to form a homotrimer (Figure 3a) with a total buried surface area of 10980 Å^2 (31% of the total solvent-accessible surface area) as determined by PISA.[48] As indicated by the sequence alignment with human arginase I, SmARG contains a 20-residue extension at the N-terminus and a 13-residue extension at the C-terminus, and a 12-residue insertion in the loop connecting α-helix B and β-strand 3.[15] The N-terminal extension (17 residues with the hexahistidine tag and its linker segment) and the inserted loop lack clearly defined electron density and are presumed to be disordered. Most of the C-terminal extension is fully ordered and contains two additional short α-helices previously unobserved in the crystal structures of arginases from other species. The S-shaped C-terminus is suggested to be important for oligomerization and mediates 54% of the intermonomer contact surface area in rat arginase I,[49] although mutagenesis studies suggest that mutations in the C-terminus destabilize but do not necessarily prevent the trimerization of rat arginase I or human arginase I.[50−52] The unusually long C-terminal tail of SmARG is similarly responsible for the majority of subunit−subunit interactions; the 13-residue extension alone contributes ~3900 Å^2 of total buried surface area (36% of the total buried surface area) to trimer assembly.

The structure of the binuclear manganese cluster (Figure 3b) is essentially identical to that observed in unliganded arginases from other species, such as human arginase I (Figure 3c). Each Mn^{2+} ion is coordinated in octahedral or distorted octahedral fashion by two nonprotein ligands and conserved metal binding residues. The metal-bridging nonprotein ligand is expected to be a hydroxide ion in the catalytically active state, and the Mn$^{2+}_A$-bound nonprotein ligand is interpreted as a water molecule. This is similar to the identification of nonprotein metal ligands in unliganded human arginase I,[40] *Bacillus caldovelox* arginase,[53] and *Leishmania mexicana* arginase.[54] Most other inner active site residues are conserved in SmARG, except that T135 in human arginase I is conserved as S165 in SmARG (Figure 3c).

Although Fitzpatrick and colleagues suggest that the SmARG activity is dependent on a disulfide bond formed between C291 and C332 on the basis of homology modeling,[15] no disulfide bond is observed in the crystal structure, even though the Sγ atoms of C291 and C332 are only 3.5 Å apart and no reducing agents were included in crystallization buffers (Figure S2a of the Supporting Information). It is clear, however, that SmARG activity is severely attenuated in the presence of reducing reagents such as TCEP (Figure S2b of the Supporting Information). Our modeling studies indicate that side chain torsion angle χ_2 of C291 could be rotated by 54° to allow the formation of a disulfide bond with C332. The geometry of this disulfide linkage would be classified as -RHStaple, which corresponds to the geometry of allosteric disulfide linkages that regulate protein function by triggering reversible changes in protein tertiary structure.[55] Even so, the side chain conformations of C291 and C332 would be unfavorable if this disulfide bond were formed.

To probe the functional importance of a possible disulfide linkage between C291 and C332, we prepared the C291A and C332A mutants of SmARG and measured their steady-state kinetics (Table 2). These mutants are chemically incapable of forming a covalent linkage between residues 291 and 332; notably, however, these mutants exhibit significant residual activity (~30% based on k_{cat}). Catalytic efficiencies (k_{cat}/K_M) are compromised 25-fold for C291A SmARG and only 9-fold for C332A SmARG. Thus, formation of a disulfide linkage between C291 and C332 is not required for catalysis but might be required for maximal catalytic function.

Structures of Complexes of SmARG with Simple Amino Acids. The overall structure of SmARG in each complex with the amino acid inhibitors L-ornithine, L-valine, and L-lysine is essentially identical to the structure of unliganded SmARG; the rmsds between liganded and unliganded structures are 0.17 Å for 322 Cα atoms in the SmARG−L-ornithine complex, 0.17 Å for 319 Cα atoms in the SmARG−L-valine complex, and 0.30 Å for 316 Cα atoms in the SmARG−L-lysine complex. As is evident in Figure 4, the molecular recognition of the catalytic product L-ornithine, the product analogue L-lysine, and the weak inhibitor L-valine is dominated by three direct and four water-mediated hydrogen bonds that selectively accommodate the α-amino and α-carboxyl groups of an amino acid with L-stereochemistry. This hydrogen bond network comprises the L-amino acid recognition motif, as first observed in the rat arginase I−ABH complex.[56]
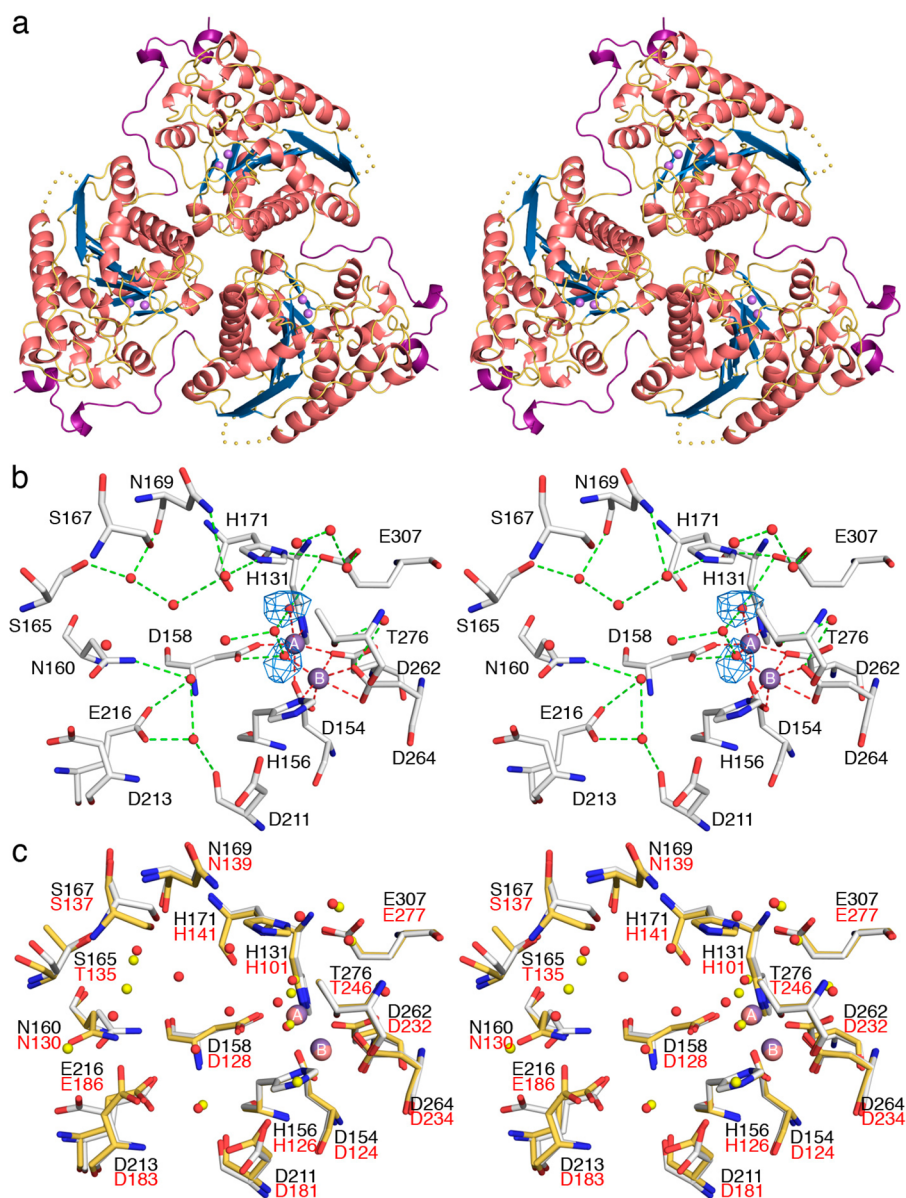
Figure 3. (a) Structure of the SmARG homotrimer. α-Helices are colored salmon, β-strands blue, and Mn^{2+} ions purple. The elongated S-shaped C-terminus is colored magenta, and the disordered K111–S119 loop appears as a yellow dotted line. (b) Simulated annealing omit map contoured at 4.0σ of the metal-bound solvent molecules in unliganded SmARG. Atoms are color-coded as follows: white for C, blue for N, red for O, purple spheres for Mn^{2+} ions, and red spheres for solvent molecules. Metal coordination and hydrogen bond interactions are represented by red and green dashed lines, respectively. (c) Superposition of unliganded SmARG (color-coded as in panel b, with black residue labels) and human arginase I (PDB entry 2ZAV; yellow for C, blue for N, red for O, pink spheres for Mn^{2+} ions, and yellow spheres for solvent molecules with red residue labels).

Structures of Complexes of SmARG with *N*-Hydroxyguanidinium Inhibitors. The overall structure of the SmARG–NOHA complex is essentially identical to that of unliganded SmARG, with an rmsd of 0.23 Å for 316 Cα atoms. The α-amino and α-carboxyl groups of NOHA hydrogen bond with the L-amino acid recognition motif, and the Nη-OH group interacts with the binuclear manganese cluster (Figure 5a). Intriguingly, however, the electron density map indicates that the *N*-hydroxyguanidinium group binds with two alternative conformations. In the major conformation (refined with 75% occupancy), the Nη-OH group of NOHA displaces the metal-bridging hydroxide ion and symmetrically bridges the binuclear manganese cluster with an average $Mn^{2+}\cdots O$ coordination distance of 1.8 Å, and the Mn^{2+}_A–Mn^{2+}_B separation increases from 3.1 to 3.3 Å. The η-NH$_2$ group of NOHA is oriented

toward Mn^{2+}_A (but does not coordinate) and donates a hydrogen bond to E307. This conformation is similar to that observed in the 2.9 Å resolution crystal structure of the rat arginase I–NOHA complex (PDB entry 1HQF).[57]

In the minor conformation (refined with 25% occupancy), the Nη-OH group of NOHA displaces the Mn^{2+}_A-bound water molecule with an average $Mn^{2+}_A\cdots O$ coordination distance of 2.0 Å. The metal-bridging hydroxide ion must also be displaced to accommodate NOHA binding in this conformation, so both Mn^{2+}_A and Mn^{2+}_B exhibit square bipyramidal coordination geometry. Two hydrogen bonds are observed between SmARG and NOHA in its minor conformation: the Nη-H group of NOHA donates a hydrogen bond to D158, and the η-NH$_2$ group donates a hydrogen bond to T276. These interactions are similar to those observed in the 2.04 Å resolution crystal
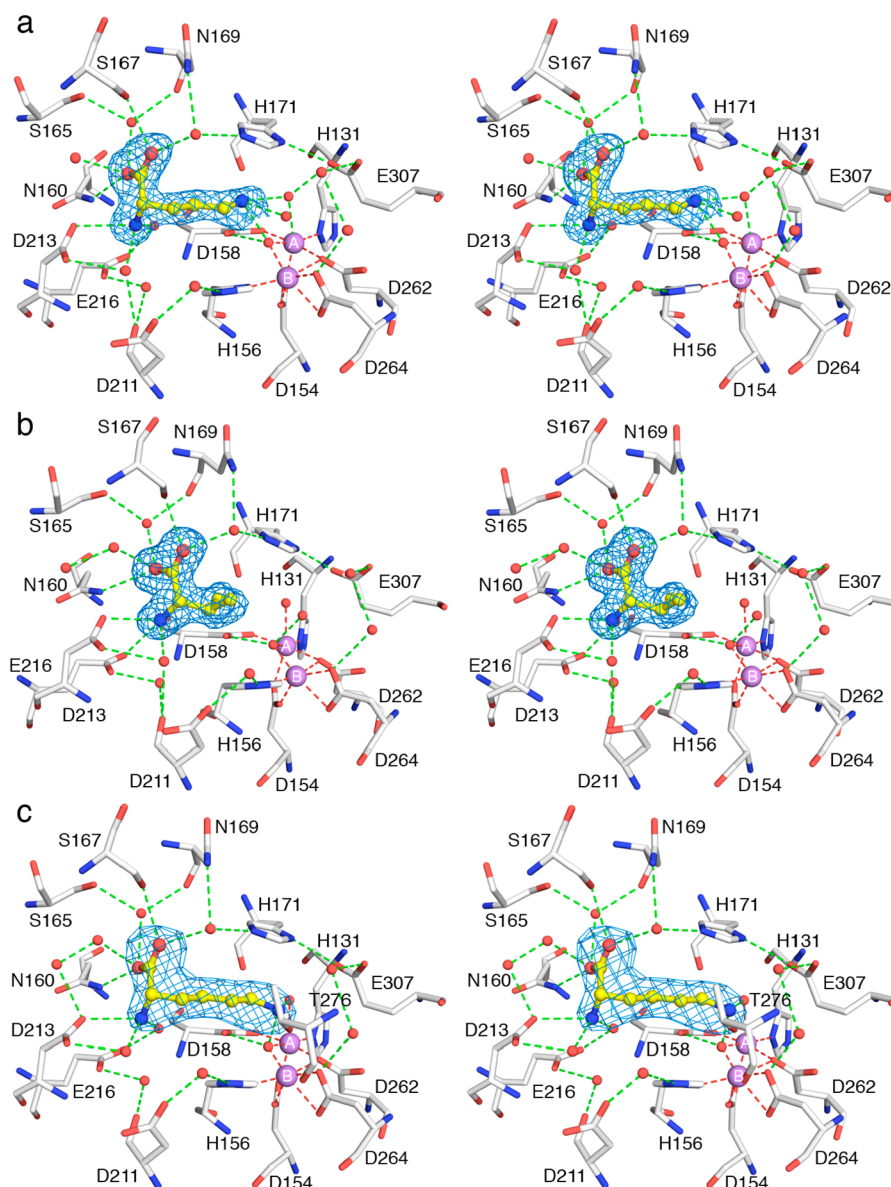
Figure 4. Simulated annealing omit maps of amino acids bound in the active site of SmARG: (a) L-ornithine, contoured at 3.0σ; (b) L-valine, contoured at 3.0σ; and (c) L-lysine, contoured at 5.5σ. Atoms are color-coded as follows: white (protein) or yellow (inhibitor) for C, blue for N, red for O, green for B, purple spheres for Mn^{2+} ions, and red spheres for solvent molecules. Metal coordination and hydrogen bond interactions are represented by red and green dashed lines, respectively. The α-amino and α-carboxyl groups of each amino acid make an array of direct and water-mediated hydrogen bonds with conserved protein residues D213, E216, N160, S165, S167, N169, and H171. These residues comprise the L-amino acid recognition motif.

structure of the human arginase I−NOHA complex (PDB entry 3LP7) (Figure S3 of the Supporting Information).[47]

Finally, the overall structure of SmARG in its complex with nor-NOHA is essentially identical to that of unliganded SmARG, with an rmsd of 0.19 Å for 331 Cα atoms. The amino acid moiety of nor-NOHA is accommodated by the L-amino acid recognition motif, as observed for NOHA. However, in contrast with the binding of NOHA, the N-hydroxyguanidinium group of nor-NOHA binds with just a single conformation in which the Nζ-OH group displaces the metal-bridging hydroxide ion and bridges the binuclear manganese cluster with average $Mn_A^{2+}\cdots O$ and $Mn_B^{2+}\cdots O$ coordination distances of 1.9 and 2.2 Å, respectively (Figure 5b). The ζ-NH group of nor-NOHA donates a hydrogen bond

to D158, and the ζ-NH$_2$ group is oriented toward Mn^{2+}_B (but does not coordinate) and donates a hydrogen bond to T276.

Structures of Complexes of SmARG with Classical Boronic Acid Inhibitors. The crystal structure of the SmARG−ABH complex reveals that no significant conformational changes are triggered upon inhibitor binding, and the rmsd is 0.15 Å for 318 Cα atoms in comparison with the unliganded enzyme. The simulated annealing omit map in Figure 6 reveals that the boronic acid group of ABH undergoes nucleophilic attack, presumably by the metal-bridging hydroxide ion of the native enzyme, to form the tetrahedral boronate anion, which mimics the tetrahedral intermediate and its flanking transition states in the arginase reaction.[30] The α-carboxylate group and α-amino group of ABH hydrogen bond with the L-amino acid recognition motif, as first observed in the
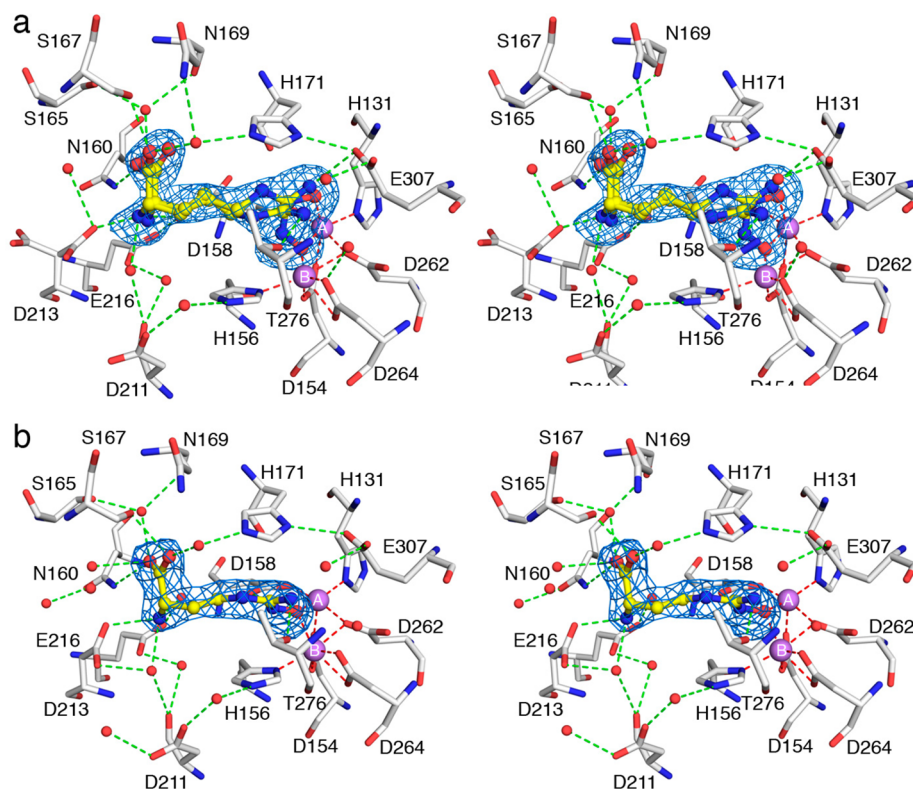
Figure 5. (a) Simulated annealing omit map (contoured at 3.0σ) of the inhibitor NOHA that reveals that the hydroxyguanidinium group adopts two alternate conformations. Atoms are color-coded as in Figure 4. Metal coordination and hydrogen bond interactions are represented by red and green dashed lines, respectively. Note that residue D213 adopts two alternate conformations. (b) Simulated annealing omit map (contoured at 3.0σ) of the inhibitor nor-NOHA. Atoms are color-coded as in Figure 4. Metal coordination and hydrogen bond interactions are represented by red and green dashed lines, respectively.
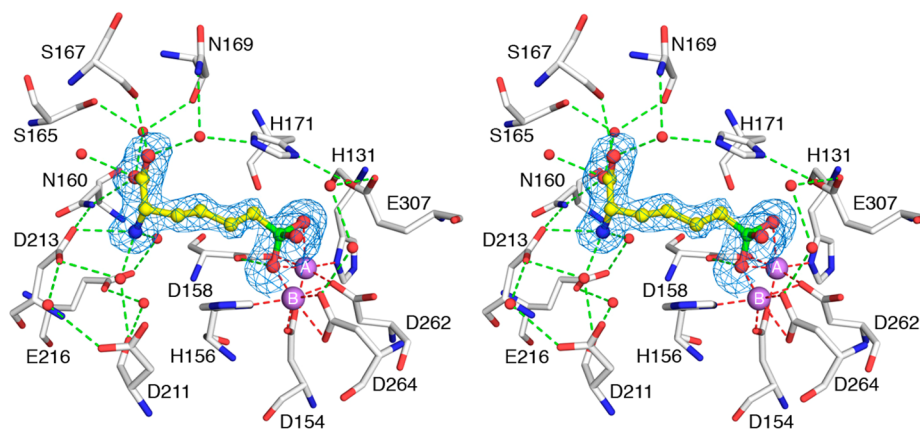

Figure 6. Simulated annealing omit map (contoured at 3.0σ) of boronic acid inhibitor ABH. Atoms are color-coded as in Figure 4. Metal coordination and hydrogen bond interactions are represented by red and green dashed lines, respectively.

crystal structure of the rat arginase I−ABH complex.[56] This structure serves as a starting point for understanding structure−activity relationships for α,α-disubstituted ABH derivatives described below.

The crystal structure of the SmARG−BEC complex, although determined at a lower resolution of 2.7 Å, similarly reveals the binding of the tetrahedral boronate anion and an array of hydrogen bonds with the α-amino acid moiety (Figure S4 of the Supporting Information). No significant conformational changes are triggered upon inhibitor binding, and the rmsd is 0.26 Å for 320 Cα atoms in comparison with the unliganded enzyme. Although fewer water molecules are

observed in the active site because of the modest resolution, the structure of the SmARG−BEC complex is similar to that first observed in the rat arginase I−BEC complex.[31]

Structures of Complexes of SmARG with α,α-Disubstituted Boronic Acid Inhibitors. The structure of the SmARG−ABH complex reveals that the Cα-H group of ABH can be substituted with an additional side chain capable of making additional interactions on the protein surface. To demonstrate the proof of concept, we have determined the crystal structures of SmARG complexes with the novel α,α-disubstituted amino acid inhibitors ABH$_{PE}$ and ABH$_{DP}$ (Figure 1b). The overall structures of SmARG complexed with ABH$_{PE}$

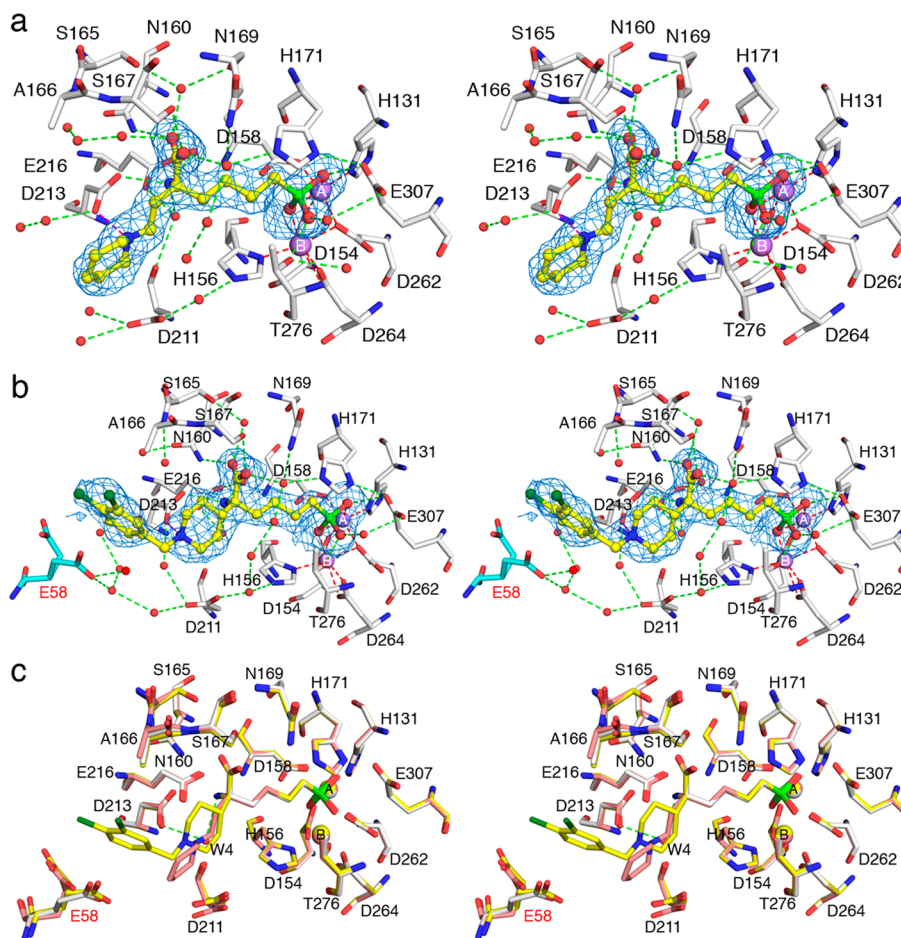**Figure 7.** Simulated annealing omit maps of α,α-disubstituted amino acid inhibitors: (a) ABH$_{PE}$, contoured at 5.0σ, and (b) ABH$_{DP}$, contoured at 3.0σ. Atoms are color-coded as in Figure 4 (dark green for Cl). Metal coordination and hydrogen bond interactions are represented by red and green dashed lines, respectively. Note that residue E58 from an adjacent monomer of the homotrimer adopts two alternate conformations (highlighted in cyan). (c) Superposition of the SmARG–ABH complex (white for C and Mn^{2+}), the SmARG–ABH$_{PE}$ complex (salmon for C and Mn^{2+}), and the SmARG–ABH$_{DP}$ complex (yellow for C and Mn^{2+}).

and ABH$_{DP}$ are essentially identical to the structure of unliganded SmARG, with rmsds of 0.19 Å for 332 Cα atoms and 0.17 Å for 330 Cα atoms, respectively. Although racemic ABH$_{DP}$ was used in the crystallization experiment with SmARG, the electron density map clearly shows that the stereoisomer corresponding to L-ABH binds exclusively in the active site. As shown in Figure 7, the boronic acid moiety of each inhibitor undergoes nucleophilic attack by the metal-bridging hydroxide ion to form a tetrahedral boronate anion, as observed in the crystal structure of the parent SmARG–ABH complex (Figure 6). However, in contrast with the SmARG–ABH complex, the additional α-substituents of ABH$_{PE}$ and ABH$_{DP}$ block the binding of water molecule W4; this water molecule ordinarily mediates a hydrogen bond between the inhibitor α-amino group and D213 (Figure 7c). Therefore, the L-amino acid recognition motif in the active site of SmARG is slightly compromised by the binding of α,α-disubstituted amino acid inhibitors. Regardless, the additional α-substituents of both ABH$_{PE}$ and ABH$_{DP}$ make additional interactions in the active site of SmARG, which presumably accounts for the affinity of these inhibitors being higher than that of ABH.

In each enzyme–inhibitor complex, the piperidine ring exclusively adopts a chair conformation and its protonated tertiary amino group donates a hydrogen bond to D213 (purple dashed lines in panels a and b of Figure 7; average N···O

separations of 2.7 Å in the SmARG–ABH$_{PE}$ complex and 2.9 Å in the SmARG–ABH$_{DP}$ complex). Additionally, the dichlorobenzyl group of ABH$_{DP}$ interacts with E58 from an adjacent monomer (panels b and c of Figure 7). Incomplete electron density for the dichlorobenzyl group of ABH$_{DP}$ and a higher average temperature factor ($\sim$55 Å^2) compared with that of the piperidine ring ($\sim$30 Å^2) suggest increased flexibility.

Structural comparison of the SmARG–ABH$_{PE}$ complex with the 1.30 Å resolution crystal structure of the human arginase I–ABH$_{PE}$ complex (PDB entry 4HWW)[34] reveals striking differences in the conformation of the piperidine α-substituent of ABH$_{PE}$, even though the parent ABH scaffold retains the same conformation in both structures (Figure 8a). Van Zandt and colleagues note that the piperidine ring of ABH$_{PE}$ adopts two alternate conformations in the human arginase I–ABH$_{PE}$ complex: distorted boat (66%) and chair (33%).[34] With the piperidine ring of ABH$_{PE}$ shifted farther from D183 in the human arginase I–ABH$_{PE}$ complex (D183 of human arginase I corresponds to D213 of SmARG), it makes water-mediated hydrogen bonds with D183 and D181 through water molecules W1 and W4, instead of making a direct hydrogen bond as observed in the SmARG–ABH$_{PE}$ complex. More importantly, because of the conservation of water molecule W4, the L-amino acid recognition motif is intact in the human arginase I–ABH$_{PE}$ complex.
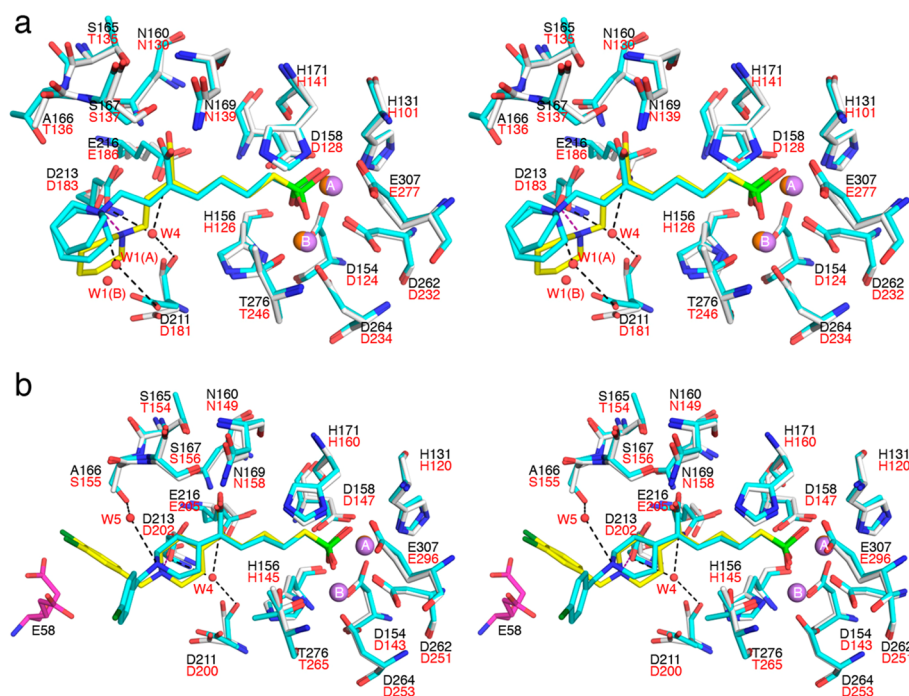
Figure 8. (a) Superposition of the SmARG−ABH$_{PE}$ complex [white (protein) or yellow (inhibitor) for C] with the human arginase I−ABH$_{PE}$ complex (cyan for C; PDB entry 4HWW). (b) Superposition of the SmARG−ABH$_{DP}$ complex [white (protein) or yellow (inhibitor) for C] with the human arginase II−ABH$_{DP1}$ complex (cyan for C; PDB entry 4IXV). Selected hydrogen bonds are shown as purple dashed lines (SmARG) or black dashed lines (human arginases). Solvent molecules are shown as small red spheres; Mn^{2+} ions are shown as purple and orange spheres in SmARG and human arginases, respectively. Black residue labels correspond to SmARG, and red labels correspond to the human arginases.

Structural differences in the binding of an α,α-disubstituted amino acid are also revealed in the comparison of the SmARG−ABH$_{DP}$ complex with the complex between human arginase II and (R)-2-amino-6-borono-2-[1-(4-chlorobenzyl)-piperidin-4-yl]hexanoate (ABH$_{DP1}$, which differs from ABH$_{DP}$ by one chlorine atom on the pendant aromatic ring; PDB entry 4IXV)[35] (Figure 8b). Here, too, the parent ABH structures adopt similar conformations; however, significant conformational differences are observed for the additional α-substituents of ABH$_{DP}$ and ABH$_{DP1}$. The piperidine ring of ABH$_{DP1}$ in the human arginase II−ABH$_{DP1}$ complex adopts a distorted boat conformation, with the piperidine amino group forming a water-mediated hydrogen bond with S155 (equivalent to T136 in human arginases I and II), instead of hydrogen bonding with D213, as observed in the SmARG−ABH$_{DP1}$ complex. Additionally, the chlorobenzyl ring of ABH$_{DP1}$ does not interact with the protein.

Active site comparisons reveal that A166 (equivalent to T136 in human arginase I and S155 in human arginase II) is another nonconserved residue in SmARG (besides S165) that can interact with α,α-disubstituted amino acid inhibitors (Figure 8). Interestingly, the corresponding residue is similarly nonpolar in two other parasitic arginases: P228 in *Plasmodium falciparum* arginase[58] and V149 in *L. mexicana* arginase.[54] Differences in polarity and size at this position between parasitic arginases and human arginases may be a contributing factor to the alternative binding modes of α,α-disubstituted amino acid inhibitors.

Coculture of Schistosomula with ABH, NOHA, and nor-NOHA. The helminth fluorescence bioassay was utilized to assess the effect of SmARG inhibitors on schistosomula viability during continuous *in vitro* cocultivation. Despite the ability of these inhibitors to effectively bind to SmARG, no significant difference in parasite viability or morphology was observed

during treatment with 100 μM ABH, NOHA, or nor-NOHA for 24 h (Figure S5 of the Supporting Information) or 72 h (data not shown). If the uptake of amino acid inhibitors is facile, this result suggests that any effect of SmARG inhibitors on parasite viability would require the presence of the human host.

■ DISCUSSION

Biological Insight into SmARG as a Drug Target for Schistosomiasis. Using a 37632-element long-oligonucleotide DNA microarray, new *S. mansoni* anthelmintic drug targets were revealed through parasite life cyle transcriptomic profiling.[45] Here, we show that one putative drug target, SmARG,[15] is maximally expressed in all life stages that interact with the definitive mammalian host but minimally expressed in life stages that interact with the intermediate snail host (Figure 2). These data confirm previously published semiquantitative reverse transcription PCR data and indicate that the upregulation of SmARG is specific to human infection by *S. mansoni*. Curiously, however, SmARG is not secreted by cercariae or schistosomula,[15] so the influence of *S. mansoni* infection on L-arginine concentrations in infected human tissues presumably arises from the facile transport of L-arginine into the parasite. The resultant depletion of host L-arginine pools allows immune evasion, because depressed L-arginine concentrations can result in lower NO concentrations produced by classically activated macrophages with known anti-schistosomula function.[59]

In principle, then, the inhibition of SmARG might possibly render the parasite more susceptible to host immunity during infection. Consistent with this hypothesis, the classical arginase inhibitors ABH, NOHA, and nor-NOHA do not affect parasite viability in the absence of the host (Figure S5 of the Supporting

Information). The host immune response *in vivo* is presumably required for the maximal anthelmintic effect of an arginase inhibitor, as is the case for praziquantel.[60]

Inhibitor Design Strategy for SmARG. Although the affinities of the classical arginase inhibitors ABH, NOHA, and nor-NOHA are in the low micromolar range (Table 2), it is somewhat surprising that these affinities fall short of the nanomolar binding affinities reported for complexes with human arginase I.[16,47] The structural basis of the weaker affinity is not clear on the basis of analysis of the crystal structures, because each inhibitor makes essentially identical metal coordination and hydrogen bond interactions in the active site of SmARG compared with the active sites of mammalian enzymes. It is clear, however, that the best inhibitors of arginase from any species will bear side chains capable of metal ion coordination. This accounts for the generally weaker binding affinity of simple amino acids such as L-valine, L-ornithine, and L-lysine, which do not interact directly with the active site Mn^{2+} ions (Figure 4). Parenthetically, we note that this feature facilitates release of the L-ornithine product during catalysis.

The crystal structures of complexes of SmARG with ABH and nor-NOHA reveal that the tetrahedral boronate anion and the *N*-hydroxyguanidinium moiety serve as ideal functional groups for metal ion coordination and active site hydrogen bond interactions (Figures 5b and 6). The α-carboxylate and α-amino group of each inhibitor also make an array of hydrogen bond interactions with the L-amino acid recognition motif, and these hydrogen bonds similarly make an important contribution to enzyme−inhibitor affinity.[61] Thus, in the quest to improve SmARG−inhibitor affinity and selectivity, these conserved features of enzyme−inhibitor recognition cannot be perturbed.

Inspection of the crystal structure of the SmARG−ABH complex (Figure 6) revealed that the L-amino acid moiety is oriented such that the Cα-H group could be substituted with a longer side chain to generate an α,α-disubstituted amino acid capable of maintaining active site interactions with its "L-side chain" while engaging in new interactions on the protein surface with its "D-side chain". The binding of ABH_{PE} and ABH_{DP} (Figure 7) with 2- and 5-fold higher affinity, respectively (Figure S1 of the Supporting Information), demonstrates the success of this strategy. Furthermore, structural comparisons of the region that accommodates the D-side chains of ABH_{PE} and ABH_{DP} indicate that this region, designated the "D-cleft" or "T136 region",[62] differs between SmARG and human arginase I. Specifically, the D-cleft of SmARG is much more nonpolar and perhaps would better accommodate hydrophobic D-side chains even longer than that of ABH_{DP}. Therefore, α,α-disubstituted amino acid inhibitors based on the ABH or nor-NOHA scaffoldings with D-side chains even more extensive than that of ABH_{DP} could be designed to further enhance binding affinity as well as selectivity against SmARG. Future studies in this regard will be reported in due course.

ASSOCIATED CONTENT

Ⓢ Supporting Information

Isothermal titration calorimetry data for SmARG−inhibitor complexes, simulated annealing omit map of C291 and C332 in unliganded SmARG, superposition of the SmARG−NOHA complex with the human arginase I−NOHA complex, simulated annealing omit map of the SmARG−BEC complex,

and helminth fluorescence bioassay data. This material is available free of charge via the Internet at http://pubs.acs.org.

Accession Codes

The atomic coordinates and structure factors have been deposited in the Protein Data Bank: unliganded SmARG, 4Q3P; SmARG−ABH complex, 4Q3Q; SmARG−ABH$_{PE}$ complex, 4Q3S; SmARG−ABH$_{DP}$ complex, 4Q3R; SmARG−BEC complex, 4Q3V; SmARG−NOHA complex, 4Q3T; SmARG−nor-NOHA complex, 4Q3U; SmARG−L-ornithine complex, 4Q42; SmARG−L-lysine complex, 4Q41; SmARG−L-valine complex, 4Q40.

AUTHOR INFORMATION

Corresponding Author

*Telephone: (215) 898-5714. Fax: (215) 573-2112. E-mail: chris@sas.upenn.edu.

ABBREVIATIONS

ABH, 2(S)-amino-6-boronohexanoic acid; ABH$_{DP}$, (R)-2-amino-6-borono-2-[1-(3,4-dichlorobenzyl)piperidin-4-yl]-hexanoic acid; ABH$_{DP1}$, (R)-2-amino-6-borono-2-[1-(4-chlorobenzyl)piperidin-4-yl]hexanoate; ABH$_{PE}$, (R)-2-amino-6-borono-2-[2-(piperidin-1-yl)ethyl]hexanoic acid; BEC, S-(2-boronoethyl)-L-cysteine; EPPS, 4-(2-hydroxyethyl)piperazine-1-propanesulfonic acid; ITC, isothermal titration calorimetry; NOHA, *N*-hydroxy-L-arginine; nor-NOHA, nor-*N*-hydroxy-L-arginine; PDB, Protein Data Bank; rmsd, root-mean-square deviation; TCEP, tris(2-carboxyethyl)phosphine hydrochloride.

REFERENCES

(1) Hotez, P. J., Savioli, L., and Fenwick, A. (2012) Neglected tropical diseases of the Middle East and North Africa: Review of their prevalence, distribution, and opportunities for control. *PLoS Neglected Trop. Dis. 6* (2), e1475.

(2) Pavlin, B. I., Kozarsky, P., and Cetron, M. S. (2012) Acute pulmonary schistosomiasis in travelers: Case report and review of the literature. *Travel Medicine and Infectious Disease 10*, 209−219.

(3) Gryseels, B. (2012) Schistosomiasis. *Infectious Disease Clinics of North America 26*, 383−397.

(4) Hams, E., Aviello, G., and Fallon, P. G. (2013) The schistosoma granuloma: Friend or foe? *Front. Immunol. 4*, 89.

(5) Pearce, E. J., and MacDonald, A. S. (2002) The immunobiology of schistosomiasis. *Nat. Rev. Immunol. 2*, 499−511.

(6) Wynn, T. A., Thompson, R. W., Cheever, A. W., and Mentink-Kane, M. M. (2004) Immunopathogenesis of schistosomiasis. *Immunol. Rev. 201*, 156−167.

(7) Anthony, B. J., Ramm, G. A., and McManus, D. P. (2012) Role of resident liver cells in the pathogenesis of schistosomiasis. *Trends Parasitol. 28*, 572−579.

(8) Greenberg, R. M. (2005) Are Ca^{2+} channels targets of praziquantel action? *Int. J. Parasitol. 35*, 1−9.

(9) Cioli, D., Botros, S. S., Wheatcroft-Francklow, K., Mbaye, A., Southgate, V., Tchuenté, L.-A. T., Pica-Mattoccia, L., Troiani, A. R., el-Din, S. H. S., Sabra, A.-N. A., Albin, J., Engels, D., and Doenhoff, M. J. (2004) Determination of ED_{50} values for praziquantel in praziquantel-resistant and -susceptible *Schistosoma mansoni* isolates. *Int. J. Parasitol. 34*, 979−987.

(10) Pica-Mattoccia, L., Doenhoff, M. J., Valle, C., Basso, A., Troiani, A.-R., Liberti, P., Festucci, A., Guidi, A., and Cioli, D. (2009) Genetic analysis of decreased praziquantel sensitivity in a laboratory strain of *Schistosoma mansoni*. *Acta Trop. 111*, 82−85.

(11) Wang, W., Wang, L., and Liang, Y. S. (2012) Susceptibility or resistance of praziquantel in human schistosomiasis: A review. *Parasitol. Res. 111*, 1871−1877.

(12) Greenberg, R. M. (2013) New approaches for understanding mechanisms of drug resistance in schistosomes. *Parasitology 140*, 1534−1546.

(13) Senft, A. W. (1963) Observations on amino acid metabolism of *Schistosoma mansoni* in a chemically defined medium. *Ann. N.Y. Acad. Sci. 113*, 272−288.

(14) Senft, A. W. (1966) Studies in arginine metabolism by schistosomes. I. Arginine uptake and lysis by *Schistosoma mansoni*. *Comp. Biochem. Physiol. 18*, 209−216.

(15) Fitzpatrick, J. M., Fuentes, J. M., Chalmers, I. W., Wynn, T. A., Modolell, M., Hoffmann, K. F., and Hesse, M. (2009) *Schistosoma mansoni* arginase shares functional similarities with human orthologs but depends upon disulphide bridges for enzymatic activity. *Int. J. Parasitol. 39*, 267−279.

(16) Di Costanzo, L., Sabio, G., Mora, A., Rodriguez, P. C., Ochoa, A. C., Centeno, F., and Christianson, D. W. (2005) Crystal structure of human arginase I at 1.29-Å resolution and exploration of inhibition in the immune response. *Proc. Natl. Acad. Sci. U.S.A. 102*, 13058−13063.

(17) Cama, E., Colleluori, D. M., Emig, F. A., Shin, H., Kim, S. W., Kim, N. N., Traish, A., Ash, D. E., and Christianson, D. W. (2003) Human arginase II: Crystal structure and physiological role in male and female sexual arousal. *Biochemistry 42*, 8445−8451.

(18) Colleluori, D. M., Morris, S. M., Jr., and Ash, D. E. (2001) Expression, purification, and characterization of human type II arginase. *Arch. Biochem. Biophys. 389*, 135−143.

(19) Sabio, G., Mora, A., Rangel, M. A., Quesada, A., Marcos, C. F., Alonso, J. C., Soler, G., and Centeno, F. (2001) Glu-256 is a main structural determinant for oligomerisation of human arginase I. *FEBS Lett. 501*, 161−165.

(20) James, S. L., and Glaven, J. (1989) Macrophage cytotoxicity against schistosomula of *Schistosoma mansoni* involves arginine-dependent production of reactive nitrogen intermediates. *J. Immunol. 143*, 4208−4212.

(21) Kropf, P., Herath, S., Weber, V., Modolell, M., and Muller, I. (2003) Factors influencing *Leishmania major* infection in IL-4-deficient BALB/c mice. *Parasite Immunol. 25*, 439−447.

(22) Roberts, S. C., Tancer, M. J., Polinsky, M. R., Gibson, K. M., Heby, O., and Ullman, B. (2004) Arginase plays a pivotal role in polyamine precursor metabolism in *Leishmania*. Characterization of gene deletion mutants. *J. Biol. Chem. 279*, 23668−23678.

(23) Gaur, U., Roberts, S. C., Dalvi, R. P., Corraliza, I., Ullman, B., and Wilson, M. E. (2007) An effect of parasite-encoded arginase on the outcome of murine cutaneous leishmaniasis. *J. Immunol. 179*, 8446−8453.

(24) Gobert, A. P., McGee, D. J., Akhtar, M., Mendz, G. L., Newton, J. C., Cheng, Y., Mobley, H. L. T., and Wilson, K. T. (2001) *Helicobacter pylori* arginase inhibits nitric oxide production by eukaryotic cells: A strategy for bacterial survival. *Proc. Natl. Acad. Sci. U.S.A. 98*, 13844−13849.

(25) Zabaleta, J., McGee, D. J., Zea, A. H., Hernandez, C. P., Rodriguez, P. C., Sierra, R. A., Correa, P., and Ochoa, A. C. (2004)

Helicobacter pylori arginase inhibits T cell proliferation and reduces the expression of the TCR ζ-chain (CD3ζ). *J. Immunol. 173*, 586−593.

(26) Rodriguez, P. C., Zea, A. H., Culotta, K. S., Zabaleta, J., Ochoa, J. B., and Ochoa, A. C. (2002) Regulation of T cell receptor CD3ζ chain expression by L-arginine. *J. Biol. Chem. 277*, 21123−21129.

(27) Rodriguez, P. C., Zea, A. H., DeSalvo, J., Culotta, K. S., Zabaleta, J., Quiceno, D. G., Ochoa, J. B., and Ochoa, A. C. (2003) L-Arginine consumption by macrophages modulates the expression of CD3ζ chain in T lymphocytes. *J. Immunol. 171*, 1232−1239.

(28) Rodriguez, P. C., Quiceno, D. G., Zabaleta, J., Ortiz, B., Zea, A. H., Piazuelo, M. B., Delgado, A., Correa, P., Brayer, J., Sotomayor, E. M., Antonia, S., Ochoa, J. B., and Ochoa, A. C. (2004) Arginase I production in the tumor microenvironment by mature myeloid cells inhibits T-cell receptor expression and antigen-specific T-cell responses. *Cancer Res. 64*, 5839−5849.

(29) Raber, P., Ochoa, A. C., and Rodriguez, P. C. (2012) Metabolism of L-arginine by myeloid-derived suppressor cells in cancer: Mechanisms of T cell suppression and therapeutic perspectives. *Immunol. Invest. 41*, 614−634.

(30) Baggio, R., Elbaum, D., Kanyo, Z. F., Carroll, P. J., Cavalli, R. C., Ash, D. E., and Christianson, D. W. (1997) Inhibition of Mn^{2+}_2-arginase by borate leads to the design of a transition state analogue inhibitor, 2(*S*)-amino-6-boronohexanoic acid. *J. Am. Chem. Soc. 119*, 8107−8108.

(31) Kim, N. N., Cox, J. D., Baggio, R. F., Emig, F. A., Mistry, S. K., Harper, S. L., Speicher, D. W., Morris, S. M., Ash, D. E., Traish, A., and Christianson, D. W. (2001) Probing erectile function: *S*-(2-Boronoethyl)-L-cysteine binds to arginase as a transition state analogue and enhances smooth muscle relaxation in human penile corpus cavernosum. *Biochemistry 40*, 2678−2688.

(32) Daghigh, F., Fukuto, J. M., and Ash, D. E. (1994) Inhibition of rat liver arginase by an intermediate in NO biosynthesis, N^G-hydroxy-L-arginine: Implications for the regulation of nitric oxide biosynthesis by arginase. *Biochem. Biophys. Res. Commun. 202*, 174−180.

(33) Custot, J., Moali, C., Brollo, M., Boucher, J. L., Delaforge, M., Mansuy, D., Tenu, J. P., and Zimmermann, J. L. (1997) The new α-amino acid N^ω-hydroxy-nor-L-arginine: A high-affinity inhibitor of arginase well adapted to bind to its manganese cluster. *J. Am. Chem. Soc. 119*, 4086−4087.

(34) Van Zandt, M. C., Whitehouse, D. L., Golebiowski, A., Ji, M. K., Zhang, M., Beckett, R. P., Jagdmann, G. E., Ryder, T. R., Sheeler, R., Andreoli, M., Conway, B., Mahboubi, K., D'Angelo, G., Mitschler, A., Cousido-Siah, A., Ruiz, F. X., Howard, E. I., Podjarny, A. D., and Schroeter, H. (2013) Discovery of (*R*)-2-amino-6-borono-(2-(2-piperidin-1-yl)ethyl)hexanoic acid and congeners as highly potent inhibitors of human arginases I and II for treatment of myocardial reperfusion injury. *J. Med. Chem. 56*, 2568−2580.

(35) Golebiowski, A., Whitehouse, D., Beckett, R. P., Van Zandt, M., Ji, M. K., Ryder, T. R., Jagdmann, E., Andreoli, M., Lee, Y., Sheeler, R., Conway, B., Olczak, J., Mazur, M., Czestkowski, W., Piotrowska, W., Cousido-Siah, A., Ruiz, F. X., Mitschler, A., Podjarny, A., and Schroeter, H. (2013) Synthesis of quaternary α-amino acid-based arginase inhibitors via the Ugi reaction. *Bioorg. Med. Chem. Lett. 23*, 4837−4841.

(36) Archibald, R. M. (1945) Colorimetric determination of urea. *J. Biol. Chem. 157*, 507−518.

(37) Otwinowski, Z., and Minor, W. (1997) Processing of X-ray diffraction data collected in oscillation mode. *Methods Enzymol. 276*, 307−326.

(38) McCoy, A. J., Grosse-Kunstleve, R. W., Storoni, L. C., and Read, R. J. (2005) Likelihood-enhanced fast translation functions. *Acta Crystallogr. D61*, 458−464.

(39) Collaborative Computational Project, Number 4 (1994) The CCP4 suite: Programs for protein crystallography. *Acta Crystallogr. D50*, 760−763.

(40) Di Costanzo, L., Pique, M. E., and Christianson, D. W. (2007) Crystal structure of human arginase I complexed with thiosemicarbazide reveals an unusual thiocarbonyl μ-sulfide ligand in the binuclear manganese cluster. *J. Am. Chem. Soc. 129*, 6388−6389.

(41) Adams, P. D., Afonine, P. V., Bunkóczi, G., Chen, V. B., Davis, I. W., Echols, N., Headd, J. J., Hung, L.-W., Kapral, G. J., Grosse-Kunstleve, R. W., McCoy, A. J., Moriarty, N. W., Oeffner, R., Read, R. J., Richardson, D. C., Richardson, J. S., Terwilliger, T. C., and Zwart, P. H. (2010) PHENIX: A comprehensive Python-based system for macromolecular structure solution. *Acta Crystallogr. D66*, 213−221.

(42) Emsley, P., Lohkamp, B., Scott, W. G., and Cowtan, K. (2010) Features and development of Coot. *Acta Crystallogr. D66*, 486−501.

(43) Laskowski, R. A., MacArthur, M. W., Moss, D. S., and Thornton, J. M. (1993) PROCHECK: A program to check the stereochemical quality of protein structures. *J. Appl. Crystallogr. 26*, 283−291.

(44) Kabsch, W., and Sander, C. (1983) Dictionary of protein secondary structure: Pattern recognition of hydrogen-bonded and geometrical features. *Biopolymers 22*, 2577−2637.

(45) Fitzpatrick, J. M., Peak, E., Perally, S., Chalmers, I. W., Barrett, J., Yoshino, T. P., Ivens, A. C., and Hoffmann, K. F. (2009) Anti-schistosomal intervention targets identified by lifecycle transcriptomic analyses. *PLoS Neglected Trop. Dis. 3*, e543.

(46) Peak, E., Chalmers, I. W., and Hoffmann, K. F. (2010) Development and validation of a quantitative, high-throughput, fluorescent-based bioassay to detect schistosoma viability. *PLoS Neglected Trop. Dis. 4*, e759.

(47) Di Costanzo, L., Ilies, M., Thorn, K. J., and Christianson, D. W. (2010) Inhibition of human arginase I by substrate and product analogues. *Arch. Biochem. Biophys. 496*, 101−108.

(48) Krissinel, E., and Henrick, K. (2007) Inference of macro-molecular assemblies from crystalline state. *J. Mol. Biol. 372*, 774−797.

(49) Kanyo, Z. F., Scolnick, L. R., Ash, D. E., and Christianson, D. W. (1996) Structure of a unique binuclear manganese cluster in arginase. *Nature 383*, 554−557.

(50) Lavulo, L. T., Sossong, T. M., Brigham-Burke, M. R., Doyle, M. L., Cox, J. D., Christianson, D. W., and Ash, D. E. (2001) Subunit-subunit interactions in trimeric arginase: Generation of active monomers by mutation of a single amino acid. *J. Biol. Chem. 276*, 14242−14248.

(51) García, D., Uribe, E., Lobos, M., Orellana, M. S., and Carvajal, N. (2009) Studies on the functional significance of a C-terminal S-shaped motif in human arginase type I: Essentiality for cooperative effects. *Arch. Biochem. Biophys. 481*, 16−20.

(52) Mora, A., del Ara Rangel, M., Fuentes, J. M., Soler, G., and Centeno, F. (2000) Implications of the S-shaped domain in the quaternary structure of human arginase. *Biochim. Biophys. Acta 1476*, 181−190.

(53) Bewley, M. C., Jeffrey, P. D., Patchett, M. L., Kanyo, Z. F., and Baker, E. N. (1999) Crystal structures of *Bacillus caldovelox* arginase in complex with substrate and inhibitors reveal new insights into activation, inhibition and catalysis in the arginase superfamily. *Structure 7*, 435−448.

(54) D'Antonio, E. L., Ullman, B., Roberts, S. C., Dixit, U. G., Wilson, M. E., Hai, Y., and Christianson, D. W. (2013) Crystal structure of arginase from *Leishmania mexicana* and implications for the inhibition of polyamine biosynthesis in parasitic infections. *Arch. Biochem. Biophys. 535*, 163−176.

(55) Schmidt, B., Ho, L., and Hogg, P. J. (2006) Allosteric disulfide bonds. *Biochemistry 45*, 7429−7433.

(56) Cox, J. D., Kim, N. N., Traish, A. M., and Christianson, D. W. (1999) Arginase-boronic acid complex highlights a physiological role in erectile function. *Nat. Struct. Biol. 6*, 1043−1047.

(57) Cox, J. D., Cama, E., Colleluori, D. M., Pethe, S., Boucher, J.-L., Mansuy, D., Ash, D. E., and Christianson, D. W. (2001) Mechanistic and metabolic inferences from the binding of substrate analogues and products to arginase. *Biochemistry 40*, 2689−2701.

(58) Dowling, D. P., Ilies, M., Olszewski, K. L., Portugal, S., Mota, M. M., Llinás, M., and Christianson, D. W. (2010) Crystal structure of arginase from *Plasmodium falciparum* and implications for L-arginine depletion in malarial infection. *Biochemistry 49*, 5600−5608.

(59) James, S. L., and Glaven, J. (1989) Macrophage cytotoxicity against schistosomula of *Schistosoma mansoni* involves arginine-dependent production of reactive nitrogen intermediates. *J. Immunol. 143*, 4208−4212.

(60) Karanja, D. M. S., Hightower, A. W., Colley, D. G., Mwinzi, P. N. M., Galil, K., Andove, J., and Secor, W. E. (2002) Resistance to reinfection with *Schistosoma mansoni* in occupationally exposed adults and effect of HIV-1 co-infection on susceptibility to schistosomiasis: a longitudinal study. *Lancet 360*, 592−596.

(61) Shishova, E. Y., Di Costanzo, L., Emig, F. A., Ash, D. E., and Christianson, D. W. (2009) Probing the specificity determinants of amino acid recognition by arginase. *Biochemistry 48*, 121−131.

(62) Ilies, M., Di Costanzo, L., Dowling, D. P., Thorn, K. J., and Christianson, D. W. (2011) Binding of α,α-disubstituted amino acids to arginase suggests new avenues for inhibitor design. *J. Med. Chem. 54*, 5432−5443.

(63) D'Antonio, E. L., Hai, Y., and Christianson, D. W. (2012) Structure and function of non-native metal clusters in human arginase I. *Biochemistry 51*, 8399−8409.

(64) Riley, E., Roberts, S. C., and Ullman, B. (2011) Inhibition profile of *Leishmania mexicana* arginase reveals differences with human arginase I. *Int. J. Parasitol. 41*, 545−552.